



A comprehensive investigation on onshore and underwater soils using CPTU and DMT tests: a case study in Yangtze River at Jiangsu, China

Xuening Liu^{1,2} · Huan He¹ · Guojun Cai^{1,2} · Guochao Zhang³ · Wen Shi¹ · Songyu Liu¹

Received: 5 July 2022 / Accepted: 3 September 2023 / Published online: 20 October 2023
© The Author(s), under exclusive licence to Springer-Verlag GmbH Germany, part of Springer Nature 2023

Abstract

The site investigation is a key part of the design of tunnel construction projects, as it provides accurate geotechnical parameters. A systematic site investigation, which consists of mainly in situ tests and laboratory sample tests, was conducted for the Haimen-Taicang river-crossing tunnel project on Yangtze River. This paper aims to analyze and compare the piezocone penetration testing (CPTU) and dilatometer test (DMT) results of both onshore and under-river subsoils to provide insights into the interpretation of the in-situ tests. The accuracy of well-documented interpretation methods based on CPTU and DMT was discussed. Current empirical correlations between in-situ test results and unit weight, undrained shear strength and constrained modulus of the subsoils were checked, and their site adaptability was discussed in detail. A series of site-specific correlations were derived based on the analysis of the in-situ tests and the comparison between the in situ tests interpretation and the laboratory results. In order to reduce the errors between testing locations caused by soil variability and get the consistent understanding of soil behaviors, CPTU–DMT correlations were reviewed and improved based on local testing results.

Keywords Dilatometer test (DMT) · Empirical correlation · Geotechnical investigation · Onshore and under-water soils · Piezocone penetration test (CPTU)

✉ Guojun Cai
37598086@qq.com

Xuening Liu
837450818@qq.com

Huan He
h_he@seu.edu.cn

Guochao Zhang
928975960@qq.com

Wen Shi
njsw95@163.com

Songyu Liu
liusy@seu.edu.cn

¹ Institute of Geotechnical Engineering, School of Transportation, Southeast University, 2# Southeast University Road, Jiangning District, Nanjing 211189, People's Republic of China

² School of Civil Engineering, Anhui Jianzhu University, No.292 Ziyun Road, Shushan District, Hefei 230601, People's Republic of China

³ China Railway Major Bridge Reconnaissance and Design Institute, No. 34, Hanyang Avenue, Hanyang District, Wuhan, Hubei, People's Republic of China

1 Introduction

The Haimen-Taicang river-crossing tunnel will be built to cross the Yangtze River, linking Haimen district (Nantong city, Jiangsu province) in the north and Taicang city (Suzhou city, Jiangsu province) in the south. The tunnel is located about 8 km downstream of the Su-Tong Highway Bridge, near the mouth of the Yangtze River. The underwater part of this tunnel is designed to be a dual-direction, six-lane, double-arch with a total length of 11.185 km. The onshore, open-cut parts on the southern and northern riverbanks are designed to be 920 m and 900 m, respectively. Thus, onshore and underwater subsoils are both involved in the initial geotechnical investigations prior to construction, the results of which are discussed in this paper.

The test site, which contains three parts (i.e., the northern riverbank, the southern riverbank and the riverbed of Yangtze River), is located about 35 km northwest of Shanghai. Figure 1 shows the location of the test site and the layout of in situ test points. The ground surfaces of both

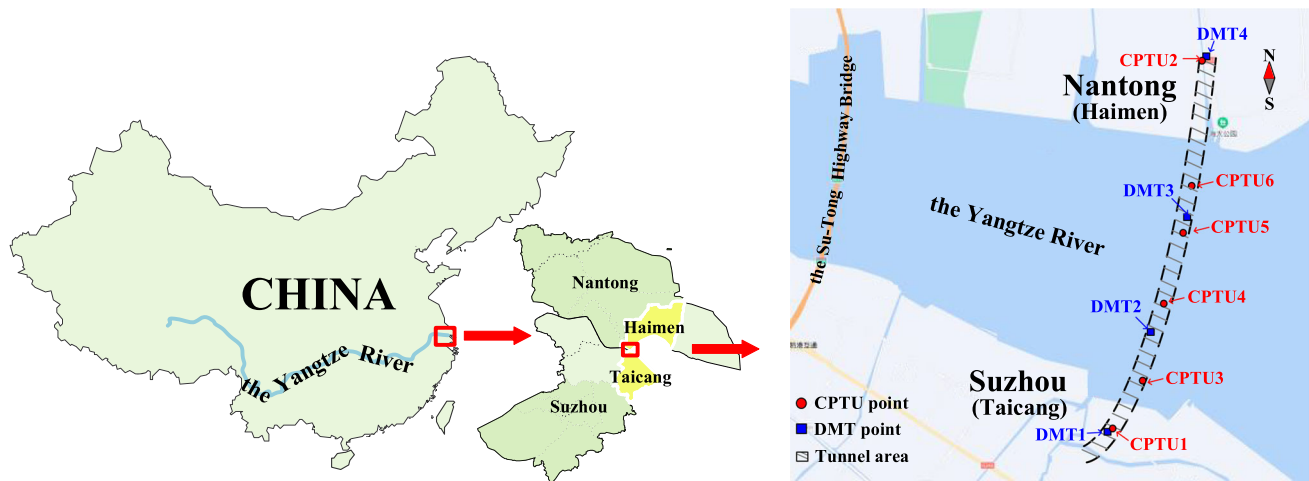


Fig. 1 Locations of sampling and in situ tests

banks are essentially flat with a level about 3.20 m (for northern bank) and 2.58 m (for southern bank) Chinese height datum (CHD). A value of 0.000 m CHD corresponds to mean sea level of the Yellow Sea for 1952–1979 measured by Qingdao tide gauge. The ground level reduces slightly towards the river.

Considering that site investigation and site characterization are of great importance in evaluating the results of the in situ and laboratory tests for design or research purposes, this study makes a comprehensive geotechnical analysis which is divided into three parts. The first part concerns the physical and mechanical properties of the soils, with the test results of both onshore and riverbed soils presented and compared. Of particular interest is the proper understanding of the mechanical behavior of underwater soft clays. Within that given geological unit, developing interrelationships between different testing data (laboratory or field) is useful to reveal correlative and statistical trends. Although some regional correlations concerning the interpretation of CPTU in the deltaic soft soils of Jiangsu Province, China, were proposed by Cai et al. [6], Duan et al. [9] and Liu et al. [15], these studies predominantly focus on onshore CPTU tests conducted on onshore soils. In the second part, taking laboratory test results as references, the accuracy of existed interpretation methods (for both CPTU and DMT) is checked, new empirical and regional correlations of soil parameters based on in situ tests for both land soils and riverbed soils are proposed. The third deals with the CPTU-DMT correlations. Even for the same geotechnical parameters, those interpreted from DMT are probably different from those interpreted by CPTU because of the different mechanism in soil failure during probe penetration. In order to get the consistent understanding of soil behaviors and compare the differences between onshore part and underwater part, several

improved CPTU-DMT correlations were provided. It is intended that the results presented will form a useful reference for engineers working on such similar sites.

2 Testing methods and results

2.1 Laboratory tests

2.1.1 Sampling and basic characterization

Index properties, as well as mechanical parameters, have been interpreted from laboratory tests performed by Southeast University (China). The clayey tube specimens obtained along the tunnel were from many continuous boreholes (located at both northern and southern banks and riverbed) drilled up to 100 m depth using a stationary piston sampler (diameter of 76 mm) and Shelby tube sampler, which for many years was the most common sampling technique used in China. The displacement method was used, where the sampler is pushed down at a constant rate to the pre-defined depth without pre-augering. The stainless steel sampling tubes of 500 mm sample length, wall thickness 1.85 mm and 7° angle of the cutting edge were employed. Figure 2 shows the sampling platform on land and river. After the withdrawal of the sampler, the tube ends were immediately sealed in situ with several layers of plastic film underlying an 8 mm-thick polystyrene plate covered externally with wax (about 12 mm thickness). In order to prevent the loss of pore water during transportation, the samples were placed vertically aligned in sealed plastic containers on a 100 mm-thick layer of wet sand as Pineda et al. [27] suggested. To minimize the disturbance caused by transportation, the gaps between tubes was infilled using scraps of polystyrene

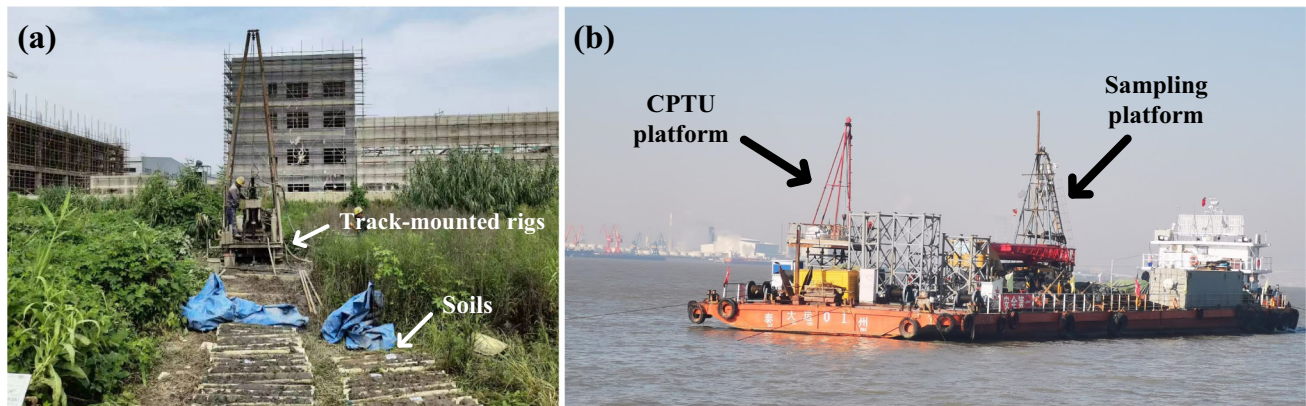


Fig. 2 Sampling methods **a** track-mounted rigs (on land); **b** floating barge (on river)

to induce lateral confinement and absorb vibrations. In order to reduce the disturbance caused by the sampling method, for each tube, top and bottom ends (2 times the sampler diameter) were used only for index tests. A preliminary characterization of the stratigraphy in the test site was obtained from the visual inspection of the geomaterials encountered during borehole drilling. The Quaternary deposits in the test site is thick, mainly containing.

Holocene artificial fill (Q_4^{ml}), alluvium (Q_4^{al}) and sea-land interactive sedimentary layer (Q_4^{mc}). Table 1 briefly summarizes the details concerning the geological stratum and the basic description of each geological unit. The whole subsurface soil stratification determined by performing linear interpolation of data from sampling boreholes is shown in Fig. 3. It can be seen from the table that within the upper -100.0 m CHD, the distribution of geological units on the north bank, south bank and the bottom of the river are not the same. There is at least one unique soil layer in each area (i.e., layer 2–1 is only found on the south bank, layer 3–2 is only found on the north bank and layer 4–4 is only found in the riverbed). Figure 3 also shows that the thickness of sandy soils on the north bank is much larger than that on the south bank. In general, the distribution of soil layers in the riverbed has high consistency with that in the south bank of the Yangtze River within the upper -50.0 m CHD, as the topsoils (layer 4–1 and layer 4–2) of riverbed extend to the south bank, but is not distributed in the north bank. As can be seen in Fig. 3 that below -50.0 m CHD, sand-like soils are dominant (layer 5–2, 5–3 and 5–4) and distributed across all three areas.

2.1.2 Testing results

The laboratory test programs included hundreds of sieve analysis tests for measuring soil particle-size distribution and index tests for measuring moisture content w , specific gravity G_s , void ratio e , unit weight γ , liquid limit w_L and

plastic limit w_p . Table 2 summarizes some basic indices of tested soils. Mechanical parameters were estimated from oedometer and triaxial tests. Constant rate of strain (CRS) oedometer tests was carried out to evaluate the compression parameters, like the compression and swell indices, C_c and C_s , the constrained modulus, M , the consolidation coefficient, c_v and the hydraulic conductivity, k_v . The undrained shear strength, S_u , was evaluated from both direct shear tests and triaxial tests, including unconsolidated undrained triaxial tests (UU) and consolidated undrained triaxial tests (CU). The specimens, during triaxial tests, were isotropically consolidated to their in situ stress state prior to undrained shearing. The values of effective vertical stress (σ'_{v0}) were obtained from index tests (depth and γ) mentioned above and the interpretation of CPTU results (i.e., using the pore water dissipation test results to get underwater level on riverbed) in the following section. Table 3 summarizes these testing results.

Comparing the test results from Table 2, the average size of particles in layer 3–1 (silty sand with silt) located in the south bank is larger than that in the north bank. The same conclusion is also available in the description of layer 5–1 (silty sand). However, for the clayey soil, the mean particle size of layer 4–2 (silty clay with silt) on the south bank is smaller than that in the north bank. It may be attributed to the orientation of the Yangtze River here, as the south bank is a sedimentary area, where large particles accumulate, and small particles are carried by water flow to the north bank. This is also the possible reason for the phenomenon that the sandy soil on the south bank is much thinner than that on the north bank, as shown in Fig. 3. Comparing the test results shown in Table 3, the mechanical properties of the same soil layer located in the south bank and riverbed are quite similar, as layer 4–1 (muddy silty clay with silt) and layer 5–1 (silty sand), whatever it is sand-like or clay-like. Although deposited depth and particle size of the same layer in both banks are close, clear differences in layer 3–1 (silty sand with silt),

Table 1 Summary of geological units

Layer no.	Thickness (m)	Soil type	Description	Distribution area
1–1	0.1–0.5	Artificial fill (Q_4^{ml})	Variegated, uneven density, asphalt concrete pavement is at 10–20 cm depth and at 20–50 cm depth is generally concrete or triad subgrade	North bank South bank
1–2	–	Silty sand with silt (Q_4^{ml+al})	Gray, full-saturated, loose, mainly composed of quartz, feldspar and mica, poorly sorted and well graded	Riverbed
2–1	1.3–3.0	Silty clay (Q_4^{al})	Gray, Grayish brown, high plasticity to medium plasticity, mixed with thin layer of silt	South bank
2–2	0.7–12.2	Silt mixed with silty clay (Q_4^{al})	Gray, medium dense, high-water-content, the thickness ratio of silty clay to silt is about 1/3.1	North bank
3–1	2.9–17.0	Silty sand with silt (Q_4^{al})	Gray and grayish yellow, medium dense, full-saturated, mainly composed of quartz, feldspar and mica, well sorted and poorly graded, locally mixed with thin layers of silt	North bank South bank
3–2	1.8–8.6	Silty sand with silty clay (Q_4^{al})	Gray, medium dense, high-water-content, the thickness ratio of silty clay to silty sand is about 1/1	North bank
4–1	1.1–8.5	Muddy silty clay with silt (Q_4^{mc})	Gray, high plasticity, with fishy smell, containing a small amount of humus, the thickness ratio of silt to muddy silty clay is about 1/2.8	South bank Riverbed
4–2	2.2–28.3	Silty clay with silt (Q_4^{mc})	Grayish brown, high plasticity to medium plasticity, silt and silty clay are interbedded, with a thickness ratio of about 1/3, containing a small amount of humus and grayish yellow ginger stone, locally mixed with a thin layer of silty sand	North bank South bank
4–3	1.6–29.6	Silt mixed with muddy silty clay (Q_4^{al})	Gray, slight dense to medium dense, high water-content, with horizontal bedding, silty clay and silt are interbedded, with a thickness ratio of about 1/2.5, locally mixed with a thin layer of silty sand	Riverbed
4–4	1.8–16.5	Silty sand with Silt (Q_4^{mc})	Grayish brown, saturated, medium dense to dense, mainly composed of quartz, feldspar and mica, well sorted and poorly graded, with horizontal bedding, silt and silty sand are interbedded, the thickness ratio is about 1/2.6, and locally mixed with thin layers of cohesive soil	South bank Riverbed
5–1	1.5–31.4	Silty sand (Q_3^{al})	Cyan gray, saturated, dense, mainly composed of quartz, feldspar and mica, well sorted, poorly graded, locally mixed with thin layer of silt	North bank South bank Riverbed
5–2	0.6–30.0	Medium-to-coarse sand (Q_3^{al+pl})	Yellowish gray and grayish yellow, saturated, dense, mainly composed of quartz, feldspar and a small amount of mica and dark minerals, poorly sorted well graded	North bank South bank Riverbed
6–1	1.2–30.9	Silty sand (Q_3^{al})	Gray, saturated, dense, mainly composed of quartz, feldspar and a small amount of mica and dark minerals, well sorted and poorly graded, locally mixed with a thin layer of medium sand and containing a small amount of calcareous cement	North bank South bank Riverbed
6–2	0.3–33.2	Medium-to-coarse sand (Q_3^{al+pl})	Yellowish gray and grayish yellow, saturated, dense, mainly composed of quartz, feldspar and a small amount of mica and dark minerals, poorly sorted, well graded	North bank South bank Riverbed
7–1	0.5–19.8	Silty sand (Q_3^{al})	Cyan grey, saturated, dense, mainly composed of quartz, feldspar and a small amount of mica and dark minerals, poorly sorted, well graded, with sporadic silty clay lenses	Riverbed
7–2	–	Medium-to-coarse sand (Q_3^{al+pl})	Yellowish gray and grayish yellow, saturated, dense, mainly composed of quartz, feldspar and a small amount of mica and dark minerals, poorly sorted, well graded. (Not penetrated through by drilling)	Riverbed

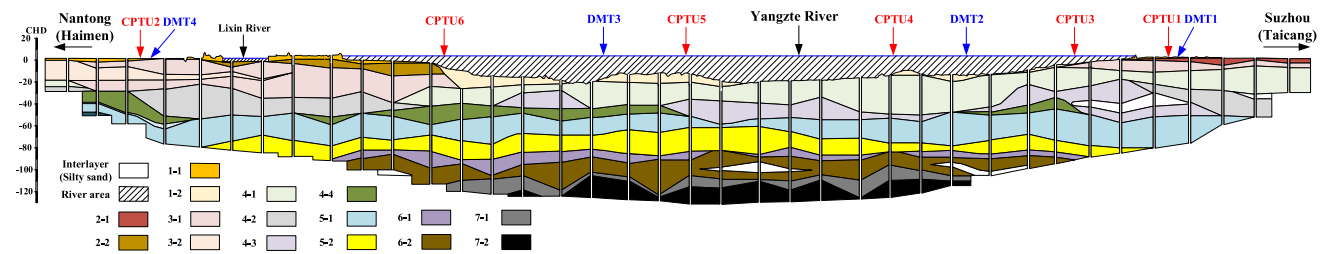


Fig. 3 Subsurface soil stratification by linear interpolation of boreholes data

layer 4–2 (silty clay with silt) and layer 5–1 (silty sand) in different river sides are observed mainly in terms of constrained modulus and consolidation coefficient.

2.2 In situ tests

2.2.1 CPTU and DMT

In order to estimate what the mechanical properties are at locations elsewhere in the sites or else depth with no samples, it is conventional to perform a high number of in situ tests relative to laboratory tests and calibrate the two kinds of data sets in order to characterize a large area of tested site reliably, rapidly and economically. The CPTU and DMT are particularly advantageous in this regard because they collect data at finer depth intervals (0.05 m and 0.5 m, respectively, in this study) comparing with other in situ tests (e.g., standard penetration test, field vane test). CPTU penetrometer is a taper-head electronic steel probe, which is penetrated into the subsoil for collecting continuous data such as cone tip resistance (q_c), sleeve friction (f_s) and pore-water pressure (u_2) of in situ sediment and transfers these data through a cable to the surface. In this study, a reference cone, which has a 10 cm² cross-sectional area and a 150 cm² sleeve area, was used. The control depth of CPTU was about 60 m with a penetration rate of 2 cm/s. Whether or not the depth reached 60 m, if the measured q_c was greater than 20 MPa or the inclination angle of the penetrometer was greater than 15°, the depth at this moment was the final depth. The in situ test programs included 6 CPTU tests, including two on the north and south banks of the Yangtze River (CPTU1 and CPTU2), respectively, and four on the river (CPTU3–CPTU6), as shown in Fig. 1. The dilatometer in this study, which was developed by Marchetti [19], is a 15 mm thick, 95 mm wide and 230 mm long flat plate with a 16° apex. A flexible stainless steel membrane with 60 mm diameter is located on the face of the blade. After the correct “A” value, which is the pressure required to begin to move the DMT membrane against the soil, and “B” value, which is the pressure required to move the center of the membrane 1.1 mm against the soil, P_0 and P_1 pressures were obtained,

respectively. Additional DMT indices can be obtained from P_0 and P_1 : (1) material index: $I_D = (P_1 - P_0)/(P_0 - u_0)$; (2) dilatometer modulus: $E_D = 34.7(P_1 - P_0)$; (3) horizontal stress index: $K_D = (P_0 - u_0)/\sigma'_{v0}$.

2.2.2 Testing river results

CPTU readings (i.e., q_c , f_s and u_2) along the depth are shown in Fig. 4. Besides, if the cone is stopped in cohesive soils exhibiting positive excess pore pressure generated during penetration, the decay of the excess pore pressure can be recorded and interpreted to provide consolidation properties. Alternatively, in sandy formations, the continuous reading of u_2 indicates the water head at that depth. The pore-water dissipation curves at specific depth are also illustrated in Fig. 4.

In the south bank, based on CPTU data, the strata can be roughly divided into four categories during the upper 50 m. The first part is from 0 to 10 m depth, which is most likely to be the layer 3–1. The main feature of this layer is the negative pore pressure measured during penetration, and the cause of this phenomenon is inconclusive, may be the partial unloading effect or the shear-induced dilatancy of overconsolidated sandy soils [3, 8]. Within the depth of 10–30 m, clayey soils are clearly identified, as the q_c and f_s are both close to zero. At the bottom of this layer, there is a pronounced jump toward 12 MPa. Below the 30 m, from the point of the larger values of q_c , sandy soils are dominate. However, the values of u_2 do not show the linear increase with depth, which is general phenomenon occurs in the clean sand. It can be inferred that the fine content of this part of sandy soils (layer 4–4, based on CHD) is large. This is also confirmed by the data in Table 2. Comparing the test results of CPTU1, 3, 4 and 5, it can conclude that, the strata of south bank and riverbed is consistent. Due to the special location of CPTU6 (i.e., the test point of CPTU6 is not located on the deep-water channel, see Fig. 3), it does not reveal the top clayey soils, which are clearly identified according to the relatively low q_c values by CPTU3, 4 and 5.

In the north bank, the variation of q_c over a wide range is mostly due to the thick silt layer interbedded with silty clay

seam which extends to 17 m (Fig. 4b). The q_c drops to a minimum of about 1.8 MPa at about 18 m (i.e., the top of layer 3–1), and then increases immediately to a high-resistance zone with the mean value of q_c is about 8.5 MPa. The consistency of the static hydraulic pressure (u_0) and u_2 indicates that, during the upper 27 m, sand is dominate in the subsurface. At the range of 27 to 32 m depth, the excess pore pressure was generated, which is indicative of the existence of fine-grained soils. However, this layer is not revealed in borehole data. Below 32 m depth, q_c , f_s and u_2 all show sharp fluctuation, which can probably be attributed to the interbedding of sandy soils and silty soils. It should be noted that given the relatively high q_c values, clayey soils are not existed below 32 m depth.

Figure 5 shows the measured results of 4 DMT tests. As expected, P_0 and P_1 increase linearly with depth whatever on land or in the riverbed. However, P_1 values show a wider variation than P_0 in all 4 tests. As mentioned above, the strata of the south bank and riverbed seem to be consistent, as the results of these tests conducted on the south bank (Fig. 5a) and on the river (Fig. 5b, c) all show a clear feature that, at 20 m depth, the material index I_D has a sharp change. Since this index is considered a single parameter in soil classification based on DMT, it is likely to be the boundary between two kinds of soils at 20 m depth, but this inference cannot be concluded in the north bank (Fig. 5d).

3 Interpretation of in situ test results and correlation analysis

3.1 Soil classification

3.1.1 Classification by CPTU

Soil classification, as one of the most important applications of CPTU test, can be conducted by various charts, which use several normalized CPTU parameters as indicators. While classifying, the CPTU data should be superimposed onto charts, which are divided into several zones representing soil types. Differ from the traditional classification methods based on grain size distribution and plasticity, and the normalized CPTU parameters reflect the mechanical behavior of the soil. Robertson [28] suggested using the following normalized CPTU parameters to identify soil behavior type (SBT) and proposed two charts based on either $Q_{t1} - F_r$ and $Q_{t1} - B_q$

$$Q_{t1} = \frac{q_t - \sigma_{v0}}{\sigma'_{v0}} \quad (1)$$

$$F_r = \frac{f_s}{q_t - \sigma_{v0}} \times 100\% \quad (2)$$

$$B_q = \frac{u_2 - u_0}{q_t - \sigma_{v0}} \quad (3)$$

where σ_{v0} = pre-penetration in-situ total vertical stress; σ'_{v0} = pre-penetration in situ effective vertical stress; u_0 = in situ equilibrium water pressure, which is resulted from the groundwater level estimated from u_2 data in each CPTU sounding by comparing the hydrostatic line to the u_2 pressure measured in sandy soil layers in pore water dissipation tests shown in Fig. 4.

Jefferies and Davies [13] identified a SBT index I_c to represent the boundaries between different soil types using $Q_{t1} - F_r$ chart, (i.e., $I_c > 2.95$ for clays, $2.05 < I_c < 2.95$ for silt mixtures and $I_c < 2.05$ for sands) as defined by

$$I_c = \sqrt{(3.47 - \log Q_{t1})^2 + (\log F_r + 1.22)^2} \quad (4)$$

Liu et al. [16] suggested that even if q_t is replaced by q_c in order to be applied to the interpretation of conventional CPT data, the $q_t - R_f$ chart from Robertson [29] was also effective.

$$R_f = (f_s/q_t) \times 100\% \quad (5)$$

This study investigated the three soil classification charts proposed by Robertson [27, 29]. The results are shown in Fig. 6 (for $q_t - R_f$ chart), 7 (for $Q_{t1} - F_r$ chart) and 8 (for $Q_{t1} - B_q$ chart).

A comparison of classification results from in situ tests and nearby boreholes at same depth is a common way to validate soil profiles interpreted from in situ tests. However, it may reveal considerable scatter due to differences in soil stratigraphy and consistency, as many sites are not uniform, and errors in depth readings are inevitable. In addition, in engineering practice, the intervals of sampling depth are generally large and thin interlayers may be ignored or merged in the thicker layers and named by the thick layer, but data measured by in situ tests are more sensitive to soil variation, it may underestimate the classification accuracy of in situ tests. Thus, during comparison, the soil sample description (Table 1) is the main calibration standard instead of the identification results given in boreholes. Although individual values at each depth could be presented in one chart, the plots become crowded and confusing with many data points. Based on this, in this section, each CPTU data profile was divided into four parts (marked by depth along with the corresponding soil layers in Fig. 3 for validation) according to close q_c values, as q_c is the most sensitive indicator of soil type among CPTU parameters.

The $q_t - R_f$ chart seems to be most reliable in soil classification on land and $Q_{t1} - B_q$ chart is most effective

Table 2 Physical properties of each geological unit in test sites

Layer no.	Items	w (%)	G_s	e	γ (kN/ m^3)	k_v (10^{-6} cm/s)	k_h (10^{-6} cm/s)	w_L (%)	w_P (%)	Particle size distribution (%)		
										> 0.25 mm	0.25– 0.075 mm	< 0.075 mm
1–2	S.Q	31	50	26	27	–	1	14	14	118	118	118
	Max	33.0	2.76	0.995	21.0	–	360	30.4	21.5	35.5	90.7	87.5
	Min	17.8	2.68	0.539	18.0	–	360	24.5	15.5	0	12.5	4.1
	Ave	25.3	2.71	0.755	19.6	–	360	27.5	19.0	5.6	55.6	38.8
2–1	S.Q	18	3	3	3	–	1	3	3	4	4	4
	Max	34.4	2.69	0.794	19.6	–	4.1	47.2	24.9	12.7	41.0	69.9
	Min	23.3	2.69	0.757	19.0	–	4.1	28.5	17.2	5	11.3	28.5
	Ave	29.0	2.69	0.779	19.4	–	4.1	34.7	21.7	7.8	28.6	63.6
2–2	S.Q	70	83	64	64	3	4	95	95	88	88	88
	Max	39.0	2.76	1.111	20.7	18.26	19.87	34.3	22.2	60.4	76.8	94.8
	Min	19.4	2.68	0.546	17.6	12.72	6.01	23.7	14.3	0	5.2	11.6
	Ave	29.3	2.69	0.850	18.9	15.92	12.30	28.6	18.7	3.7	38.5	57.8
3–1 (North)	S.Q	12	12	12	12	–	–	32	32	64	64	64
	Max	34.8	2.7	0.994	19.0	–	–	36.3	21.8	24.0	81.7	84.9
	Min	28.6	2.7	0.866	17.7	–	–	19.4	10.7	0	39.6	35.7
	Ave	31.7	2.7	0.939	18.3	–	–	25.5	14.8	3.7	40.9	51.8
3–1 (South)	S.Q	5	5	5	5	–	–	7	7	30	30	30
	Max	31.6	2.8	0.853	19.9	–	–	33.2	21.0	10.7	87.3	61.2
	Min	21.0	2.7	0.678	19.0	–	–	21.5	13.7	0	17.3	9.6
	Ave	24.6	2.7	0.764	19.4	–	–	29.2	17.8	4.6	56.5	36.4
3–2	S.Q	18	18	18	18	–	1	23	23	21	21	21
	Max	41.8	2.73	1.127	19.6	–	10.0	41.4	24.8	5.8	54.8	72.4
	Min	27.4	2.68	0.742	17.4	–	7.51	26.8	16.9	1.5	26.1	41.7
	Ave	33.9	2.70	0.983	18.3	–	8.76	33.2	19.9	3.7	46.4	49.9
4–1 (South)	S.Q	52	52	52	52	2	25	52	52	6	6	6
	Max	51.5	2.7	1.424	18.6	12.8	18	41.8	22.1	11.7	79.2	58.6
	Min	30.6	2.7	0.996	17.0	12.1	1.5	30.1	16.2	0	13	18.6
	Ave	36.8	2.7	1.077	17.8	12.4	12	34.5	19.6	6.6	39.1	48.6
4–1 (Riverbed)	S.Q	12	17	11	11	7	15	29	29	152	152	152
	Max	35.6	2.7	0.928	20.0	16.65	60	33.1	23.3	3.4	41.1	100
	Min	22.7	2.68	0.656	18.4	5	0.43	21.9	13.4	0	0	58.9
	Ave	26.3	2.69	0.731	19.5	10.9	10.03	26.9	18.2	0.1	13.9	86
4–2 (North)	S.Q	15	15	15	15	1	1	22	22	10	10	10
	Max	35.1	2.7	1.009	18.8	16.8	8.6	33.4	19.6	16	69.1	76.6
	Min	27.3	2.7	0.881	17.7	16.8	8.6	21.2	11.8	0	28.6	40.3
	Ave	31.4	2.7	0.954	18.1	16.8	8.6	28.5	16.7	11.8	32	56.2
4–2 (South)	S.Q	43	43	43	43	–	5	46	46	8	8	8
	Max	34.3	2.7	1.000	19.5	–	15.5	37.6	21.6	7.7	36	63.4
	Min	20.0	2.7	0.682	16.9	–	3.0	24.2	15.4	2.1	18.3	45.5
	Ave	28.3	2.7	0.905	18.2	–	11.1	31.0	18.4	4.6	32.4	57.8
4–3	S.Q	37	48	33	36	1	13	49	49	24	24	24
	Max	42.8	2.8	1.374	20.2	13.92	62.0	42.3	26.8	7	47.7	100
	Min	17.2	2.7	0.601	15.9	13.92	1.38	22.0	14.6	0	0	50.1
	Ave	32.1	2.7	1.017	17.7	13.92	10.93	30.5	20.7	0.4	16.6	83

Table 2 (continued)

Layer no.	Items	w (%)	G_s	e	γ (kN/ m^3)	k_v (10^{-6} cm/s)	k_h (10^{-6} cm/s)	w_L (%)	w_P (%)	Particle size distribution (%)		
										> 0.25 mm	0.25– 0.075 mm	< 0.075 mm
4–4	S.Q	21	21	24	23	–	–	28	28	19	19	19
	Max	38.8	2.8	1.179	21.2	–	–	32.6	22.7	47.9	92.3	100
	Min	17.8	2.7	0.535	17.2	–	–	17.2	10.0	0	0	1.8
	Ave	25.6	2.7	0.792	19.0	–	–	28.1	19.4	5.1	52.6	42
5–1 (North)	S.Q	61	63	47	57	–	5	–	–	5	5	5
	Max	32.6	2.7	0.917	20.9	–	1100.0	–	–	16.4	70.2	45.7
	Min	10.3	2.7	0.470	18.0	–	180.0	–	–	0.4	33.6	19.4
	Ave	21.2	2.7	0.676	19.5	–	410.0	–	–	8.7	57	34.3
5–1 (South)	S.Q	74	68	50	64	–	3	–	–	43	43	43
	Max	29.8	2.7	0.973	21.2	–	950.0	–	–	42.1	78.9	46.9
	Min	11.7	2.8	0.459	17.6	–	340.0	–	–	0	11.1	3.3
	Ave	19.8	2.8	0.660	19.4	–	496.7	–	–	20.2	55.5	23.8
5–1 (Riverbed)	S.Q	220	236	142	181	–	8	12	12	179	179	179
	Max	32.6	2.76	1.100	21.4	–	600.0	30.1	21.9	49.2	95.6	49.9
	Min	11.6	2.67	0.433	17.1	–	110.0	16.5	16.5	0	22.4	1.3
	Ave	21.2	2.70	0.694	19.5	–	408.0	19.7	19.7	12.4	60.5	27.1
5–2	S.Q	120	111	35	40	–	–	–	–	144	144	144
	Max	19.2	2.72	0.793	21.5	–	–	–	–	77.3	42.3	13.2
	Min	7.1	2.65	0.365	16.9	–	–	–	–	18.5	0.3	0
	Ave	12.1	2.67	0.530	19.7	–	–	–	–	60.2	14.7	15
6–1	S.Q	29	29	16	23	–	–	–	–	137	137	137
	Max	36.8	2.72	0.937	21.4	–	–	–	–	74.5	94.8	47
	Min	9.8	2.67	0.396	18.0	–	–	–	–	0	9.6	0
	Ave	20.0	2.69	0.659	19.4	–	–	–	–	30.7	51	22.6
6–2	S.Q	74	71	25	32	–	–	–	–	117	117	117
	Max	25.2	2.69	0.721	21.4	–	–	–	–	77.3	90.5	39.2
	Min	7.4	2.64	0.361	17.1	–	–	–	–	0	3.9	0
	Ave	12.9	2.67	0.513	19.8	–	–	–	–	60.2	17.3	14.8

S.Q. statistical quantity, *Max.*, *Min.* and *Ave.* are the maximum, minimum and mean value, respectively

–, indicates that the data is not available

in defining soils underwater after a comprehensive comparison between Figs. 6, 7 and 8 and Table 1 (Description column). This conclusion generally resulted from:

- the CPTU data are easily located out of the coordinate range in $Q_{t1} - F_r$ chart, especially for soft soils (e.g., CPTU1-②, CPTU2-④ and CPTU4-①).
- $Q_{t1} - B_q$ chart provides a poor estimate in CPTU1 and CPTU2 (both of them were performed on land). It seems to overestimate the stiffness of soils, as in CPTU1-①, -③, -④ and in CPTU2-①, -②, -④, the number of data points which inferred as sandy soils are obviously higher than the classification results obtained from other two charts, and it is also inconsistent with

the description of the corresponding soil layer in Table 2.

- Sand content suggested by $q_t - R_f$ chart seems to be overestimated in CPTU3-②, CPTU4-③, -④ and CPTU6-③ (all of these tests were conducted on the river), since these soils are mostly identified as silty sand.
- $Q_{t1} - B_q$ chart suggested a little amount of sensitive fine-grained soils exist in CPTU4-①, CPTU5-①. This is also consistent with the description in Table 1 as “muddy soils”. However, in other two charts, this kind of soils are not revealed.

Table 3 Mechanical properties of each geological unit in test sites

Layer no.	C_c	C_s	M (MPa)	c_v ($10^{-3}\text{cm}^2/\text{s}$)				c_d (kPa)	φ_d (°)	c_{uu} (kPa)	φ_{uu} (°)	c_{cu} (kPa)	φ_{cu} (°)	c' (kPa)	φ' (°)
				At 50 kPa	At 100 kPa	At 200 kPa	At 400 kPa								
2–1	0.180	0.022	4.86	5.84	5.47	5.20	3.01	17.1	14.4	20.5	8.3	18.4	18.6	19.3	19.2
2–2	0.229	0.028	15.43	6.65	5.68	5.09	3.88	11.2	13.4	10.9	13.2	21.9	26.2	25.4	27.0
3–1	–	–	16.68	6.51	5.90	5.61	3.94	15.1	13.6	21.9	18.2	26.7	31.7		
(North)															
3–1	–	–	15.11	6.23	5.74	5.45	3.20	13.6	16.3	21.2	17.0	25.3	32.4		
(South)															
3–2	–	–	6.02	6.91	6.60	6.43	3.25	18.1	13.9	18.0	14.2	29.0	26.5		
4–1	0.245	0.024	4.20	4.13	3.96	3.92	3.21	12.2	10.2	6.8	6.2	13.7	15.1	13.9	18.8
(South)															
4–1	0.193	0.014	4.33	4.81	3.62	3.51	3.80	12.5	12.5	10.9	5.0	11.5	18.9	13.6	21.9
(Riverbed)															
4–2	0.174	0.019	4.47	6.22	5.73	4.47	4.27	13.3	12.3	17.0	12.1	51.0	29.9	19.9	23.3
(North)															
4–2	0.198	0.016	11.45	6.98	6.16	5.98	4.43	15.4	13.6	18.1	17.1	26.5	22.4	17.2	20.5
(South)															
4–3	–	–	5.34	6.19	4.56	4.56	4.28	13.8	19.6	14.0	9.8	14.5	26.0	16.3	28.3
4–4	–	–	10.56	8.22	7.13	7.35	3.87	14.8	21.5	–	–	–	–		
5–1	–	–	4.44	8.20	7.27	6.96	5.53	8.9	31.3	–	–	–	–		
(North)															
5–1	–	–	6.21	7.12	6.27	6.03	5.17	9.1	33.8	–	–	–	–		
(South)															
5–1	–	–	11.76	7.47	6.55	6.45	5.18	10.4	36.5	–	–	3.6	31.6		
(Riverbed)															
5–2	–	–	12.46	–	–	–	–	5.4	41.3	–	–	–	–		
6–1	–	–	12.27	–	–	–	–	2.4	36.8	–	–	–	–		
6–2	–	–	13.48	–	–	–	–	2.2	41.0	–	–	–	–		

M is calculated at $\sigma'_{v0} = 100 \sim 200\text{kPa}$; c_d , φ_d are obtained by direct shear test; c_{uu} , φ_{uu} are obtained by UU test; c_{cu} , φ_{cu} are obtained by CU test; c' , φ' are obtained by CD test

3.1.2 Classification by DMT

According to Marchetti [19], the material index I_D was originally used as a simple and approximate parameter for identifying the soil type, i.e., $I_D \leq 0.6$ for clay, $0.6 < I_D < 1.8$ for silt and $I_D \geq 1.8$ for sand. Similar to the CPTU classification methods, I_D is a parameter reflecting the mechanical behavior (i.e., the geomaterials which are classified as clay, silt and sand based on I_D have clay-, silt- and sand-like behavior, respectively). The classification criterion is shown in Fig. 5., which shows that I_D can range from 0.1 to 10 and is commonly illustrated on a log scale. The classification method was improved adding E_D as another parameter in the classification process.

Comparing with the soil profiles shown in Fig. 3, the classification results obtained by DMT seem to provide a good estimation between sandy soils and clayey soils (Fig. 9). It should be noted that the DMT method defines the type of soil too broadly, and the data interval is larger than CPTU. DMT chart seems to be ineffective in distinguishing silt from clay (see DMT2). Based on this, if the soil stratigraphy of tested site is dominated by clay and silt interbedding, the soil classification method based on DMT will not be able to describe the soil profile at all, as the data points will be mixed together on the chart and cannot be recognized (see DMT4). Thus, it is untenable to conclude that DMT is more effective than CPTU in soil classification.

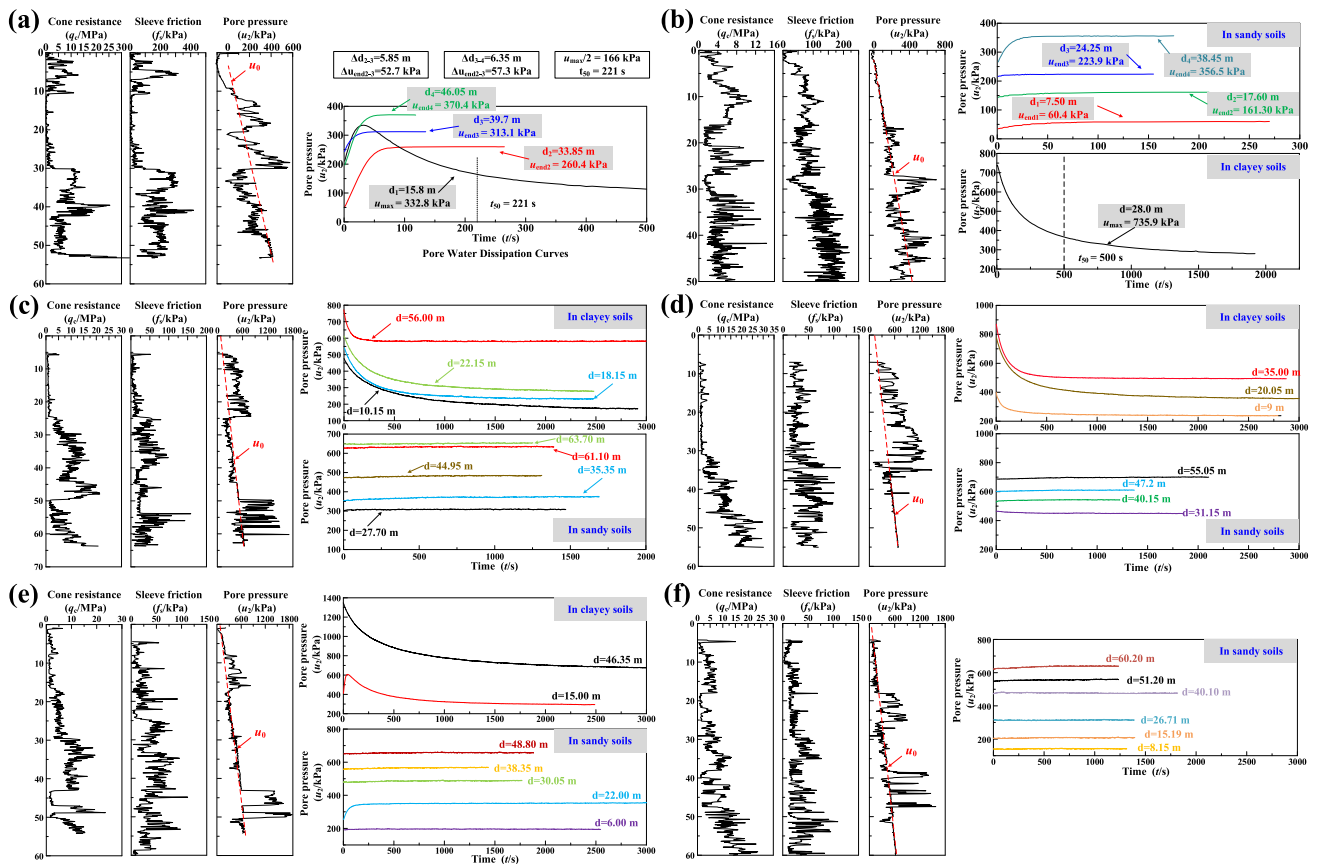


Fig. 4 CPTU results: a CPTU1; b CPTU2; c CPTU3; d CPTU4; e CPTU5; f CPTU6

3.2 Interpretation of geotechnical parameters

Empirical or semi-empirical correlations provide a simple way to estimate the physical or mechanical properties of soils using CPTU and DMT data, but the empirical coefficients included in estimation are always obtained by mathematical statistics of the laboratory test results from a given site and may not be applicable to other regions. It is well-acknowledged that these empirical correlations need to be verified when applied at a local testing area to consider the different geological histories and conditions, which have great influence on soil properties. As the proposed empirical correlations are site-specific, and few validation works were made for underwater soils, in this section, an applicability study was made to screen the appropriate correlations to interpret some physical and mechanical parameters of both land and underwater soils in tested sites based on CPTU and DMT methods. To simplify the presentation and avoid the great scatter caused by the inhomogeneity between sampling sites and in situ test sites, in each uniform soil layer, the validation works were only performed on average values of each tested soil index. Table 4 summarizes the average values of in situ test parameters for each tested soil layer.

3.2.1 Unit weight

3.2.1.1 Interpretation from CPTU Due to the indispensability in calculating overburden stress of soil layers, unit weight (γ) is a basic parameter used in interpretation of CPTU data. Lunne et al. [17] proposed empirical values of unit weight (γ_{chart}) (Table 5) for all 12 kinds of soils in q_t - R_f chart. Robertson and Cabal [31] combined correlations between shear wave velocity and soil unit weight [20], as well as DMT results and soil unit weight (Fig. 9) to link γ_{eq} with CPTU data, as defined by

$$\gamma_{eq}/\gamma_w = 0.27\log R_f + 0.36\log(q_t/p_a) + 1.236 \quad (6)$$

The unit weights obtained from Table 4 and Eq. 6 as well as γ_{lab} (taken as calibration standards), which is determined in the laboratory, are summarized in Table 5. It is obvious that whatever for onshore data (CPTU1 and CPTU2) and riverbed data (CPTU3 to CPTU6), γ_{chart} shows a better correlation with γ_{lab} than γ_{eq} .

3.2.1.2 Interpretation from DMT The soil classification chart (Fig. 9) developed by Marchetti and Crapps [23] provides direct indications about the unit weight of soils in the process of soil classification. When comparing the

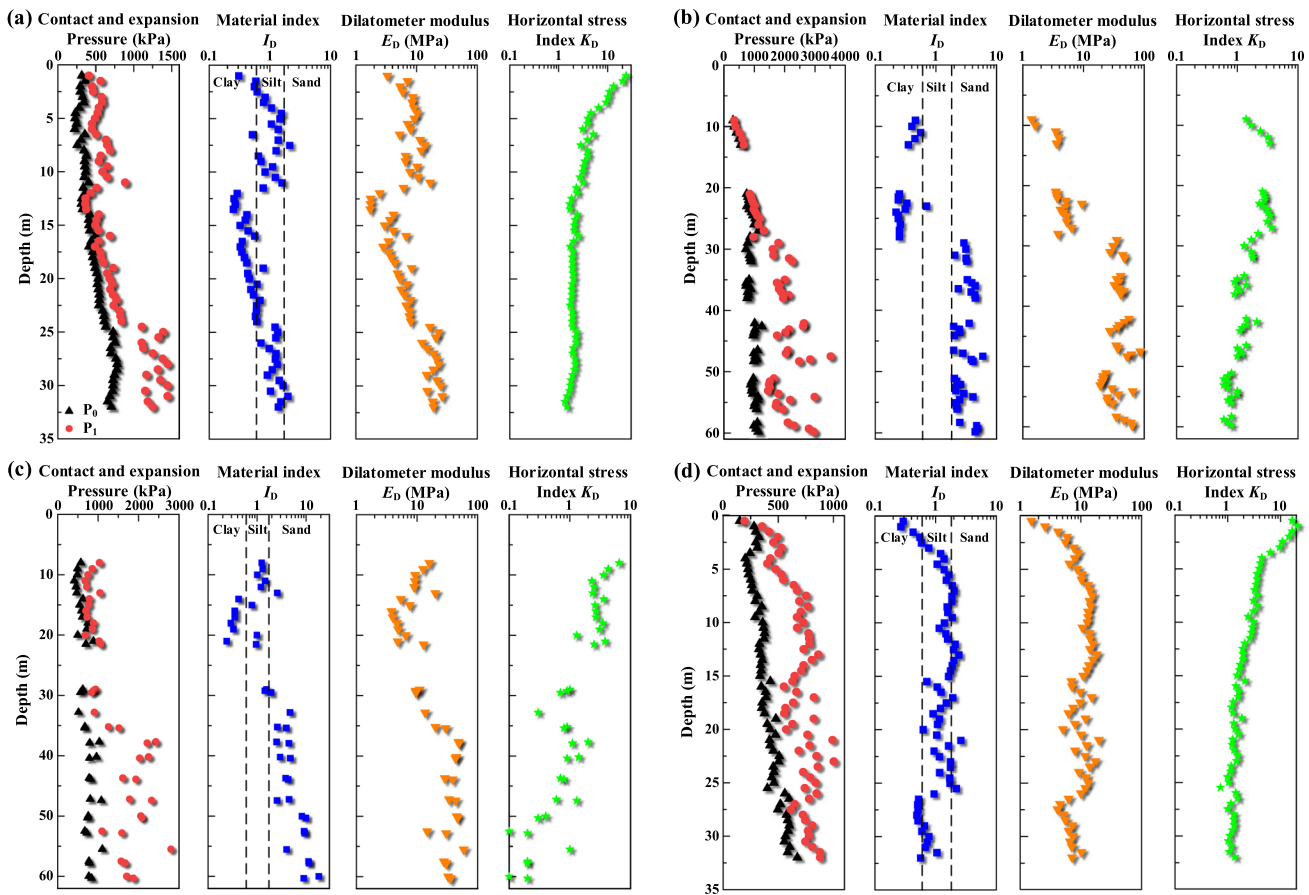


Fig. 5 DMT results: a DMT1; b DMT2; c DMT3; d DMT4

predicted γ_{chart} with γ_{lab} , it can be observed that the unit weight of each kind of soils is underestimated by the chart. In consideration of the high accuracy of Table 4 in γ estimation is only based on soil type, I_D is a single index in soil classification by DMT, there is a strong possibility that a link exists between γ and I_D . A direct relationship between γ and I_D was found by conducting a polynomial regression analysis, using semi-logarithmic scaling in Fig. 10.

The resulting equation can be expressed as

$$\gamma = 18.65 + 2.07 \log_{10} I_D - 0.94(\log_{10} I_D)^2 \quad (R^2 = 0.67) \tag{7}$$

This relationship derived from both onshore and riverbed data, and the applicability of this relationship should be validated in other sites. In addition, due to the functional properties of quadratic function, when I_D increases to 12.64, γ decreases with the increase of I_D , it is obviously not consistent with our engineering experience. Thus, Eq. 21 is only acceptable to the range: $0.1 < I_D < 12.64$.

3.2.2 Undrained shear strength (S_u)

3.2.2.1 Interpretation from CPTU A large number of empirical correlations have been reported on the interpretation of undrained shear strength of cohesive soils (i.e., layer 4–1 in this paper) from CPTU data [7, 10]. From the tip resistance in cohesive soils, the S_u profile with depth can be determined by applying the bearing capacity equation to the cone, which is commonly expressed as

$$S_u = \frac{q_t - \sigma_{v0}}{N_{kt}} \tag{8}$$

where N_{kt} is the cone bearing capacity factor, characterised by a large range of variation for different sites, commonly varies from 8 to 20 for normally consolidated clay, could approach to more than 30 for over-consolidated soils [5, 11].

An alternative derivation of undrained strength can be obtained by dividing the excess pore pressure ($\Delta u = u_2 - u_0$) by the cone pore pressure factor $N_{\Delta u}$ as suggested by Robertson et al. [30]

$$S_u = \frac{\Delta u}{N_{\Delta u}} \tag{9}$$

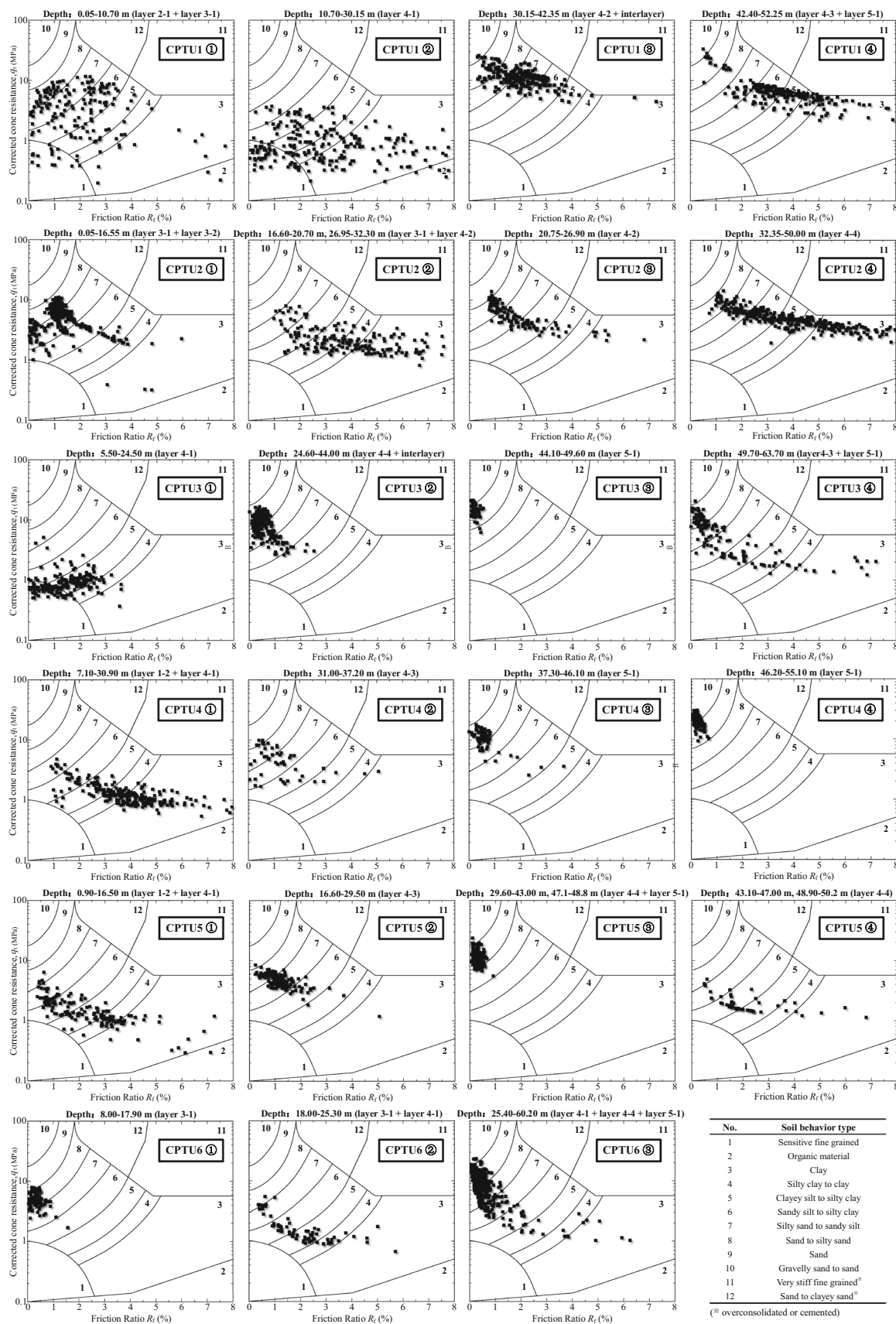


Fig. 6 Soil classification results based on CPTU using q_t-R_f chart

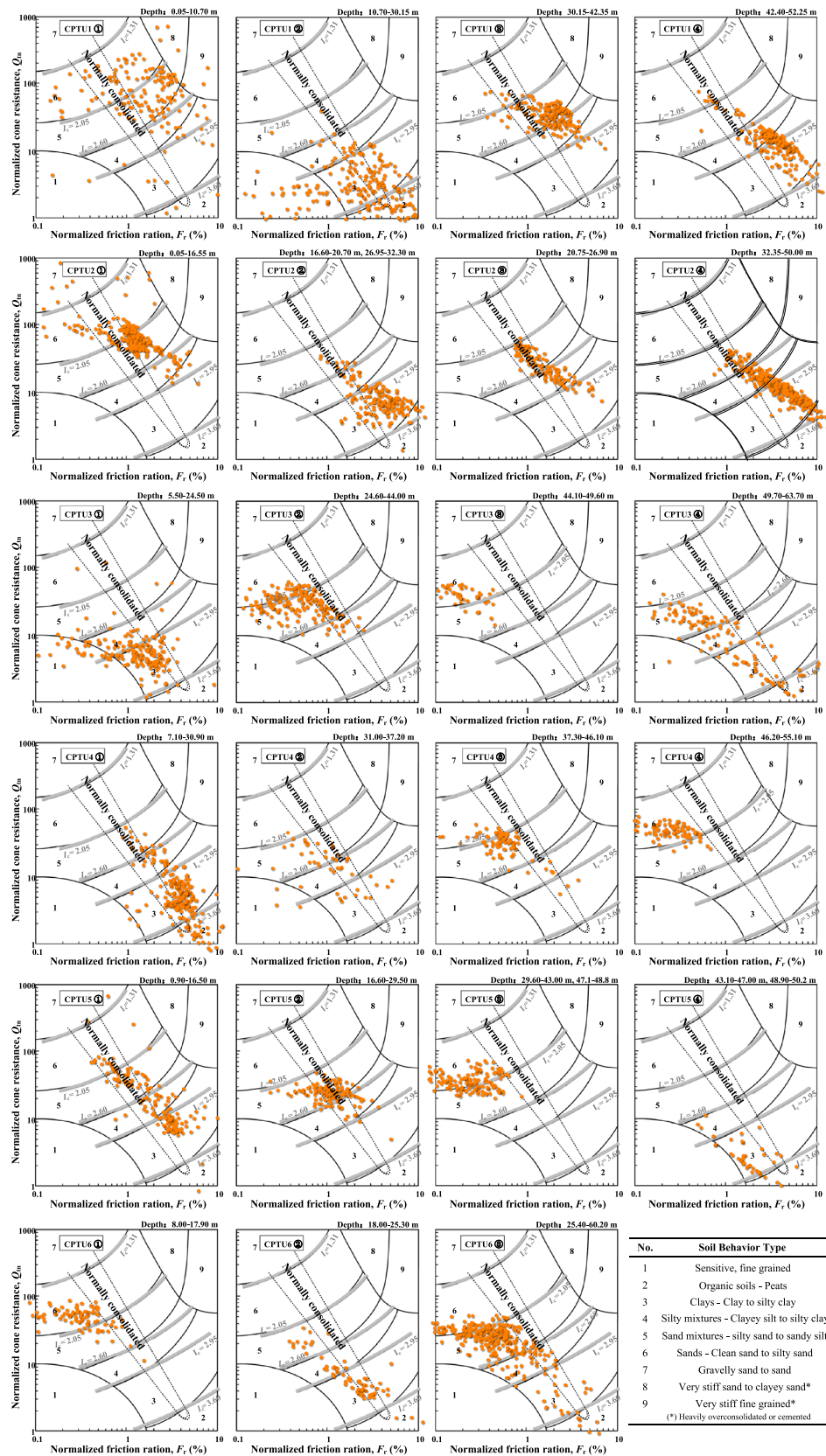


Fig. 7 Soil classification results based on CPTU using $Q_{n1}-F_r$ chart

Many attempts have been made to correlate the cone factors N_{kt} and $N_{\Delta u}$ empirically with CPTU parameters in order to obtain S_u values rapidly. Mayne [21] correlated N_{kt} and $N_{\Delta u}$ to the normalised cone pore-water factor B_q as Eq. 10,

$$\begin{cases} N_{kt} = \frac{3.90}{1 - B_q} \\ N_{\Delta u} = \frac{3.90}{1/B_q - 1} \end{cases} \quad (0.5 < B_q < 0.7) \quad (10)$$

and then, Mayne and Peuchen [22] reduced the scatter of data points in the relationship between B_q and N_{kt} by presenting the Eq. 11.

$$N_{kt} = 10.5 - 4.6 \ln(B_q + 0.1) \quad (B_q > -0.1) \quad (11)$$

Ahmed and Agaiby [2] empirically linked these two factors with I_c as Eq. 12.

$$\begin{cases} N_{kt} = 1.925I_c + 4.334 \\ N_{\Delta u} = 1.925I_c + 0.429 \end{cases} \quad (12)$$

Besides, in order to obtain S_u from CPTU tests (based on Eq. 13 provided by Vesic [32, 33]), since the measured u_2 is the parameter that shows the least variation from one type of CPTU equipment to another, if the pore-pressure measurement system is sufficiently well-saturated, Mayne [21, 22] linked rigidity index (I_R) with CPTU pore-pressure parameters, as Eqs. 14 and 15.

$$\begin{cases} N_{kt} = 4/3(\ln I_R + 1) + \pi/2 + 1 \\ N_{\Delta u} = 4/3(\ln I_R + 1) \end{cases} \quad (13)$$

$$I_R = \exp\left[\frac{2.93B_q}{1 - B_q}\right] \quad (0.5 < B_q < 0.7) \quad (14)$$

$$I_R = \exp\left[\frac{1.5 + 2.925M\left(\frac{U^* - 1}{Q}\right)}{M - M\left(\frac{U^* - 1}{Q}\right)}\right] \quad (15)$$

where $Q = (q_t - \sigma_{v0})/\sigma'_{v0}$; $U^* = (u_2 - u_0)/\sigma'_{v0}$; $M = (6 \sin \phi') / (3 - \sin \phi')$.

Table 6 summaries the results based on aforementioned methods. Except CPTU5, the N_{kt} and $N_{\Delta u}$ calculated directly from laboratory results based on Eqs. 8 and 9 varies in a narrow range. To a degree that reflects reliability of in situ data. Compared to the results directly from laboratory tests, Eqs. 10 and 12 give no consistency with them. The results from Eq. 11 show a good agreement with $N_{kt,UU}$ for riverbed soils (i.e., CPTU 3-CPTU6) and the results from Eqs. 13 and 15 show a considerable consistency with $N_{kt,CU}$ and $N_{\Delta u,CU}$. However, in the process of validating Eq. 15, the values of effective friction angle (ϕ') is also needed from laboratory. Although many researchers have provided several correlations between ϕ' and CPTU

parameters [26], no wide-accepted conclusions have been put forward so far.

3.2.2.2 Interpretation from DMT The primary correlation for determining S_u from the DMT test is provided by Marchetti (1980), in the normalised form Lutenegeger [18] expressed by the relationship:

$$S_u/\sigma'_{v0} = 0.22(0.5K_D)^{1.25} \quad (16)$$

It is meaningful to conduct site-specific verification to Eq. 16 in this study, because the constants 0.22 and 1.25 are related to overconsolidated ratio and plasticity index of investigated soils. Besides, these constants were provided using field vane test as reference test, it may inevitably introduce errors in estimation when comparing with laboratory test results. Figure 11 depicts the relationships between S_u/σ'_{v0} and K_D for the submarine clay (layer 4–1) taking DS, UU and CU test as reference test, respectively. In addition, many researchers used linear relationship directly linked S_u with DMT parameters [18], but after verification, these empirical relationships are also not applicable in this case.

3.2.3 Constrained modulus (M)

3.2.3.1 Interpretation from CPTU In geotechnical practice, settlement and stability are two primary considerations related to the design of structures on soft sites. Constrained modulus (M) is a significant parameter to estimate the magnitude of consolidation settlement of subsoils. In practice, it has been usual to linearly correlate the modulus M with net cone resistance ($q_t - \sigma_{v0}$) [14]. The measured M obtained from the one-dimensional consolidation tests were compared with net cone resistance shown in Fig. 12. This figure also presents the best fitting lines of ($q_t - \sigma_{v0}$) to measured M , as $M = 3.095(q_t - \sigma_{v0})$ for layers 4–1, 3–2 and 3–1 and $M = 1.104(q_t - \sigma_{v0})$ for layers 4–2 and 4–3. It should be noted that measured M for layers 4–4 and 5–1 seem to have weak relationship with ($q_t - \sigma_{v0}$) resulted from the large inhomogeneity in these layers, as described in Table 1.

3.2.3.2 Interpretation from DMT To estimate one-dimensional constrained modulus (M), the correlation with E_D is used in the form:

$$M_{DMT} = R_M \cdot E_D \quad (17)$$

where R_M is calculated after:

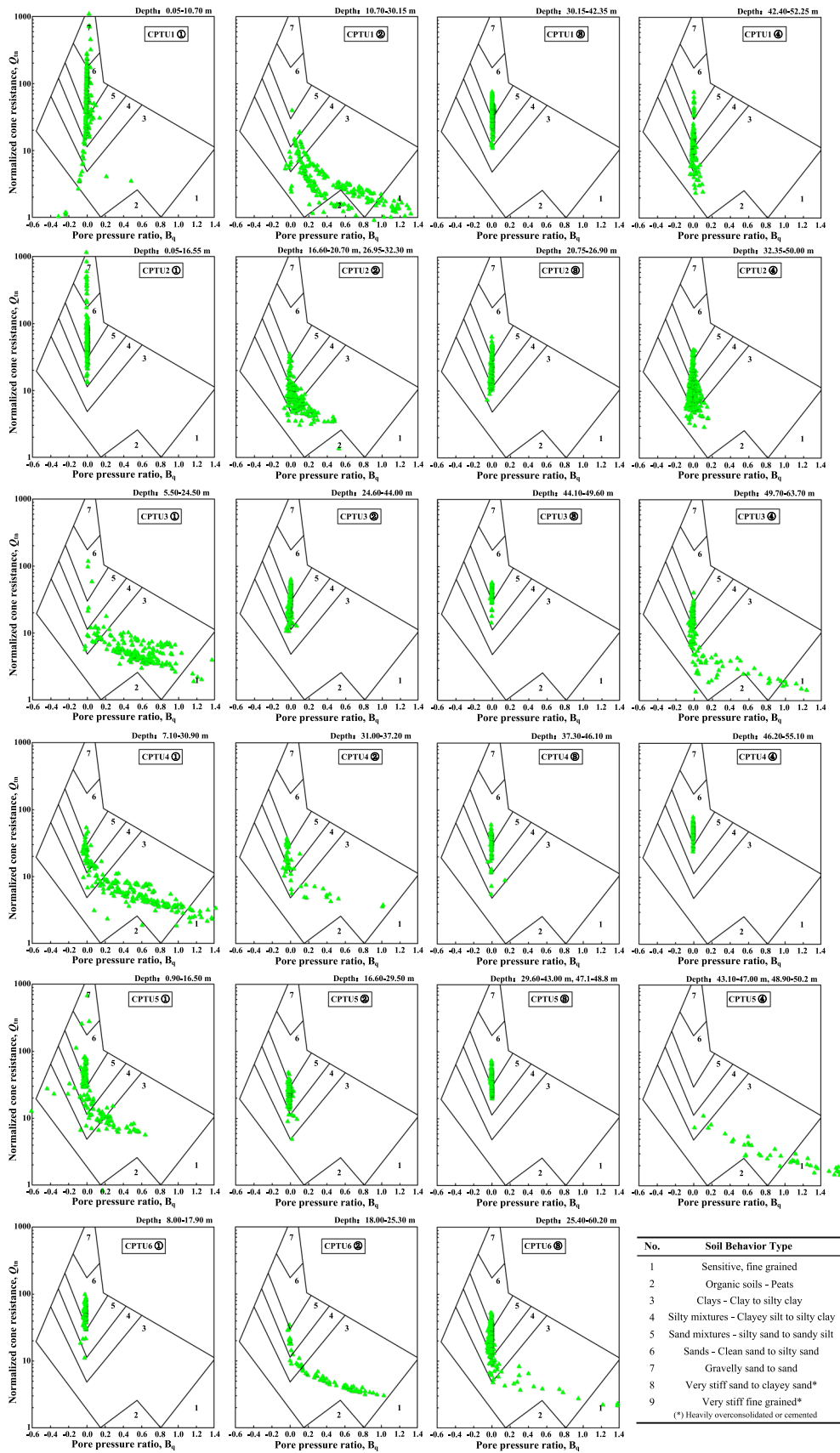


Fig. 8 Soil classification results based on CPTU using Q_{n1} - B_q chart

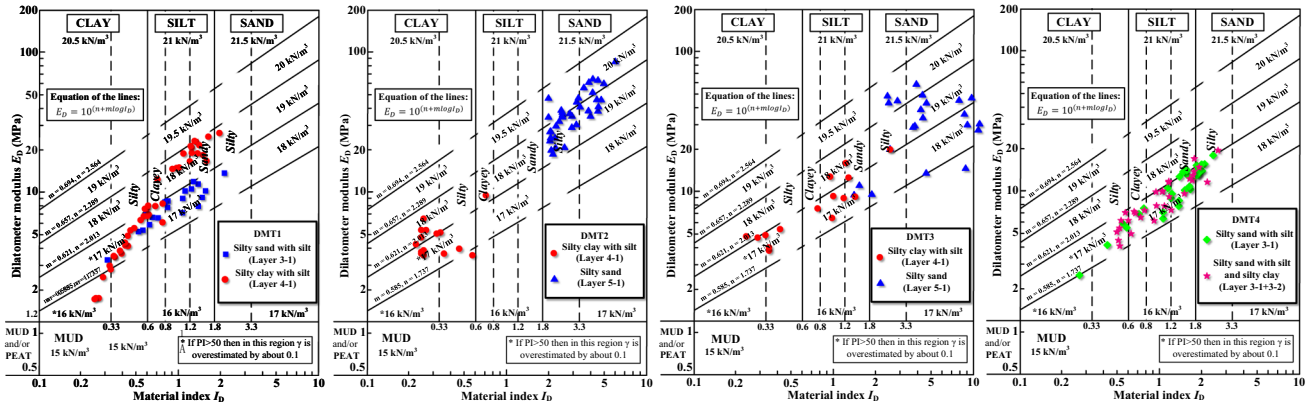


Fig. 9 Soil classification results based on DMT

Table 4 Measured data by in situ tests for each soil layer

In situ tests	Layer no.	$q_{l,ave}$ (kPa)	$R_{f,ave}$ (%)	γ_{chart} (kN/m ³)	γ_{eq} (kN/m ³)	γ_{lab} (kN/m ³)	In situ tests	Layer No	$I_{D,ave}$	$E_{D,ave}$ (MPa)	$K_{D,ave}$	γ_{chart} (kN/m ³)	γ_{lab} (kN/m ³)	
CPTU1	3–1	4910.8	2.38	18.5	19.06	19.5	DMT1	3–1	0.998	8.326	7.071	17	19.5	
	4–1	859.1	2.16	18	16.28	17.8		4–1	0.509	5.381	2.020	17*	17.8	
	Interlayer	11,442.0	2.0	19	20.16	19.1		4–2	1.264	19.393	1.911	18	17.9	
	4–3	5613.7	3.34	18	19.65	17.7		DMT2	4–1	0.338	4.353	2.765	17*	17.8
CPTU2	3–1	5323.3	1.27	19	18.46	19.3	DMT3	5–1	2.972	37.832	1.118	15	19.5	
	3–2	1968.0	3.43	18	18.08	18.3		5–2	4.660	56.633	0.700	15	19.7	
	4–2	5917.65	1.68	19	18.95	17.9		DMT3	1–2	1.463	12.683	3.600	17	19.6
	4–4	5068.5	3.36	18	19.51	19		4–1	0.523	6.056	2.867	17*	17.8	
CPTU3	4–1	967.24	0.90	18.5	15.45	17.8	DMT4	5–1	5.808	35.961	0.733	19	19.5	
	4–4	8630.8	0.52	19.5	18.18	17.7		5–2	18.280	32.600	0.010	18	19.7	
	5–1	14,743.4	0.21	20	17.95	19.5		DMT4	3–1	1.593	12.145	3.603	17	19.3
CPTU4	4–1	1381.6	2.14	18	17.00	17.8	DMT4	3–2	1.361	10.776	1.360	17	18.3	
	4–3	4848.2	0.97	19	18.01	17.7		4–2	0.631	6.469	1.217	17	17.9	
	5–1	15,388.1	0.42	20	18.82	19.5								
CPTU5	4–1	1589.0	1.71	18.5	16.95	17.8								
	4–3	4776.0	1.06	19	18.09	17.7								
	4–4	10,859.5	0.26	19.5	17.73	19								
CPTU6	3–1	5149.9	0.32	19.5	16.83	19.5								
	4–4	6281.9	1.29	19	18.73	19								
	5–1	13,802.0	0.31	20	18.30	19.5								

$$R_M = \begin{cases} 0.14 + 2.36\log K_D (I_D \leq 0.6) \\ R_{M,0} + (2.5 - R_{M,0})\log K_D (0.6 < I_D < 3) \\ 0.5 + 2\log K_D (I_D > 3) \\ 0.32 + 2.18\log K_D (K_D > 10) \\ \geq 0.85 \end{cases} \quad (18)$$

where $R_{M,0} = 0.14 + 0.15(I_D - 0.6)$. Figure 13 shows the comparison of the measured M values from the laboratory tests and the predicated values (for all layers penetrated through by DMT) based on Eqs. 17 and 18. The

determination coefficient is 0.603, indicating that the estimation method based on DMT is acceptable. If the point with large deviation (marked as layer 5–1) are excluded, the determination coefficient will increase to 0.777. It should be noted that, in Eq. 18, R_M must be larger than 0.85, but this limitation increases the deviation to laboratory results and does not be accepted in Fig. 13.

Table 5 Empirical values of unit weight in q_t - R_f chart for 12 kinds soils

Zone no.	γ_{chart} (kN/m ³)	Zone no.	γ_{chart} (kN/m ³)
1	17.5	7	18.5
2	12.5	8	19.0
3	17.5	9	19.5
4	18.0	10	20.0
5	18.0	11	20.5
6	18.0	12	19.0

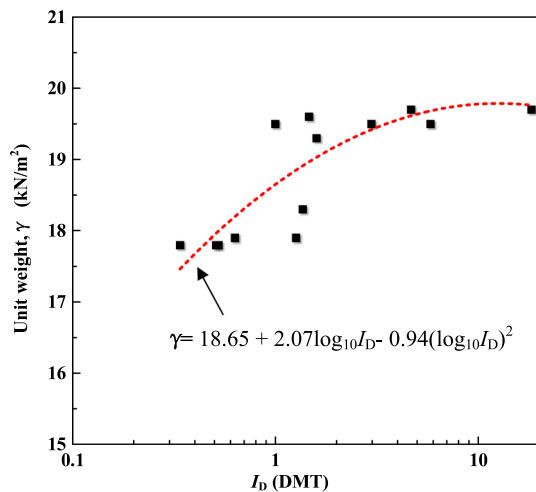


Fig. 10 Unit weight γ versus material index I_D

4 DMT–CPTU correlations

Although DMT and CPTU are popular in site investigation worldwide, neither of them measures mechanical properties of soils directly, whatever clayey soils or sandy soils, both of them can be derived based on theoretical or empirical correlations with different degree of accuracy. Most empirical correlations are site-specific, it is necessary to verify their usability before engineering practice. On the other hand, most theoretical correlations are based on cavity expansion theory. In any event, these expressions can only provide approximate interpretation results since neither DMT blade nor CPTU penetrometer with 60° apex tip are perfectly represented by an infinite cylinder nor by a perfect sphere. Thus, the two techniques both have their own advantages and disadvantages in the interpretation of geotechnical parameters. For example, Ahmadi and Robertson [1] argued that CPT penetrometer can sense a soil interface up to 15 cone diameters ahead and behind based on the stiffness of soil layers. However, DMT appears to be less influenced by ahead and behind soils since the blade is stopped during recording parameters.

What’s more, as mentioned above, DMT predicts constrained modulus presumably more inline with the laboratory results. CPT, especially CPTU, has accumulated a lot of engineering/research experiences worldwide because its high-efficiency and simple-operation and can be interpreted more geotechnical parameters than DMT. CPT has a somewhat more extensive theoretical background compared to the DMT, as well as a larger database of well-documented case histories for certain applications. It is noted that the accuracy of CPTU in soil classification has been validated globally and the continuous readings of CPTU can depict the soil profiles (especially in detecting thin interlayers) as accurately as possible. Therefore, the combined use of DMT together with CPTU can be a good complement in defining geo-stratigraphy and soil geotechnical parameters. Interrelationships between CPT and DMT data can validate, expand and improve correlations and applications by using existing engineering experience from one test and extrapolating to the other.

Comparison of intermediate DMT parameters and those derived from CPTU data after Robertson [29] and Grabar et al. [12] was made to discuss on the equivalence/non-equivalence of CPTU and DMT data. Robertson [29] pointed out that the proposed correlations are unlikely to be applicable for all soils but regarded them as framework, which is available for future refinements. Thus, in this section, it is interesting to observe the validity of the existing correlations for the study areas.

Robertson [29] presented CPT and DMT data from published records and showed a trend between I_D and I_c , defined by

$$I_c = 2.5 - 1.5 \log I_D \tag{19}$$

A comparison of readings from adjacent CPTU and DMT tests in the study area is shown in Fig. 14, reveals considerable scatter versus Eq. 19, especially for clayey soils. With the above Eq. 19 as a framework, regression analysis was conducted to obtain I_D - I_c correlation for clay-like soils. The proposed correlation is expressed as

$$I_c = \begin{cases} 2.5 - 1.5 \log I_D & (I_c > 2.95, I_D < 0.6) \\ 1.9 - 4.76 \log I_D & (I_c < 2.95, I_D > 0.6) \end{cases} \tag{20}$$

It should be noted that, for soils, which is out of the applicable conditions, for example, $I_c > 2.95, I_D > 0.6$ (i.e., DMT and CPTU do not classify these soils into the same category), Eq. 20 is ineffective to link I_D with I_c .

Overconsolidation ratio (OCR) and the coefficient of lateral earth pressure (K_0) are one of the most important parameters for geotechnical design but hard to obtain strictly whatever in field or in laboratory. In terms of CPT, OCR and K_0 are typically obtained by multiplying the net cone resistance ($q_t - \sigma_{v0}$) by an empirical coefficient, which varies along with the site type. Thus, in engineering

Table 6 Summaries of cone factor results from several methods

CPTU no.	Depth (m)	$S_{u,DS}$ (kPa)	$S_{u,UU}$ (kPa)	$S_{u,CU}$ (kPa)	$N_{kt,DS}$	$N_{kt,UU}$	$N_{kt,CU}$	N_{kt} (Eq. 10)	N_{kt} (Eq. 11)	N_{kt} (Eq. 12)	N_{kt} (Eqs. 13 and 15)
					$N_{\Delta u,DS}$	$N_{\Delta u,UU}$	$N_{\Delta u,CU}$	$N_{\Delta u}$ (Eq. 10)	$N_{\Delta u}$ (Eq. 12)	$N_{\Delta u}$ (Eqs. 13 and 15)	
1	20.5 + 0	78.6	46.9	113.3	6.5	10.9	4.5	–	4.8	11.1	4.7
					3.3	5.6	2.3	–	7.2	2.1	
3	15.1 + 5.65	85.0	39.5	123.5	6.8	14.5	4.6	10	12.1	9.9	5.7
					3.4	7.3	2.4	6.1	6.0	3.1	
4	19 + 15	120.9	53.7	178.9	5.7	12.7	3.8	–	10.4	9.6	5.8
					3.3	7.5	2.2	–	5.7	3.3	
5	8.7 + 13.5	76.5	36.2	110.4	9.9	21.0	6.9	–	15.3	9.2	4.2
					2.3	4.9	1.6	–	5.3	1.6	
6	21.7 + 7.1	114.5	51.2	169.1	6.8	15.2	4.6	7.8	12.8	9.7	4.7
					2.7	6.0	1.8	3.9	5.8	2.1	

The values in ‘Depth’ column = depth in soils + distance between the soil surface to the river surface; the values of $S_{u,DS}$, $S_{u,UU}$ and $S_{u,CU}$ are obtained by direct shear test, UU test and CU test, respectively; the values of $N_{kt,DS}$ or $N_{\Delta u,DS}$, $N_{kt,UU}$ or $N_{\Delta u,UU}$ and $N_{kt,CU}$ or $N_{\Delta u,CU}$ are calculated from Eq. 13 or Eq. 14 using $S_{u,DS}$, $S_{u,UU}$ and $S_{u,CU}$, respectively

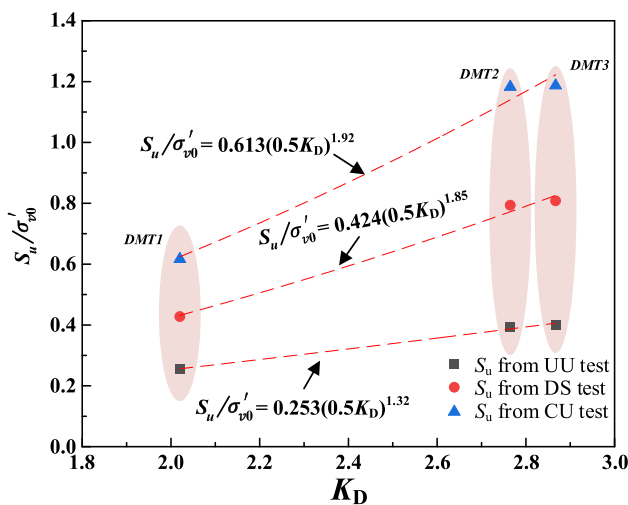


Fig. 11 Normalised undrained strength versus horizontal stress index

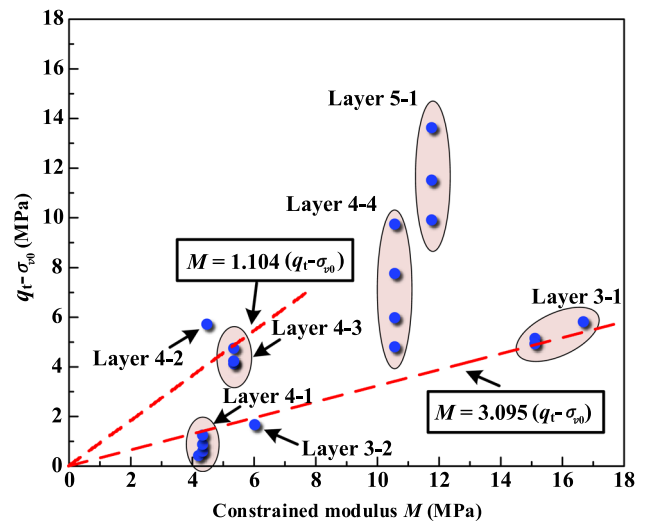


Fig. 12 Constrained modulus from laboratory tests versus $(q_t - \sigma_{v0})$

practice, whether there is a reliable value of empirical coefficient becomes the key point to evaluate OCR or K_0 using CPT. On the contrary, OCR and K_0 can be estimated directly using DMT recordings. Marchetti [19] proposed the correlations for deriving OCR and K_0 from K_D in clay are expressed as

$$OCR = (0.5K_D)^{1.56} \tag{21}$$

$$K_0 = (K_D/1.5)^{0.47} - 0.6 \tag{22}$$

In sand, CPT and DMT tests seem unable to estimate these two geotechnical parameters solely. Many efforts

have been made to estimate OCR and K_0 directly combining DMT and CPT parameters. Monaco et al. [25] derived the correlation:

$$OCR = 0.0344(M_{DMT}/q_t)^2 - 0.4174(M_{DMT}/q_t) + 2.2914 \tag{23}$$

Based on a series results of calibration chamber (CC) test, Balid et al. [4] proposed $K_0 - K_D - q_c$ correlations using simple algebraic equations:

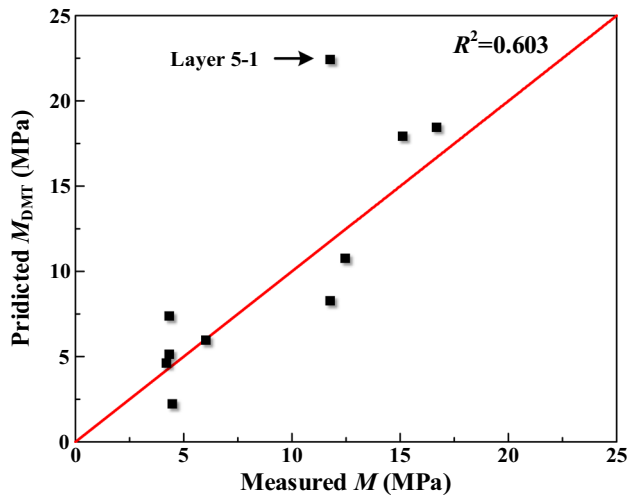


Fig. 13 Constrained modulus from laboratory tests compared with that predicted from DMT test (using Eq. 18)

$$K_0 = 0.376 + 0.095K_D - 0.0017q_c/\sigma'_{v0} \tag{24}$$

$$K_0 = 0.376 + 0.095K_D - 0.0046q_c/\sigma'_{v0} \tag{25}$$

These two equations were determined as the best fit of pluviated artificial sand and natural Po river sand, respectively. Marchetti et al. [24] approved this method and recommended the following values of the last coefficient: – 0.002 in “freshly deposited” sand, – 0.005 in “seasoned” sand. Equations 21 to 25 are the few methods available to estimate OCR and K_0 (or at least the shape of these two parameters profiles) by in situ test. Thus, in engineering practice, using CPT-DMT correlations ($Q_{t1} - K_D$ correlations in this section) can reduce the amount of workload to conduct two kinds of in situ test to take Eqs. 21 to 25 into application easily and also avoid the measurement errors caused by soil variability between different testing locations (although the distance between testing locations may be small). Robertson [29] provided $K_D - Q_{t1}$ and $E_D - Q_{t1}$ correlations, which are expressed as Eqs. 26 and 27, respectively.

$$K_D = 0.3(Q_{t1})^{0.95} + 1.05 \tag{26}$$

$$\frac{E_D}{\sigma'_{v0}} = 5Q_{t1} \tag{27}$$

A comparison of these intermediate parameters from adjacent CPTU and DMT tests in the study area is shown in Fig. 15. A similar analysis conducted on $I_D - I_c$ correlation was also performed on $K_D - Q_{t1}$ and $E_D - Q_{t1}$ correlations, and the obtained correlations are expressed as

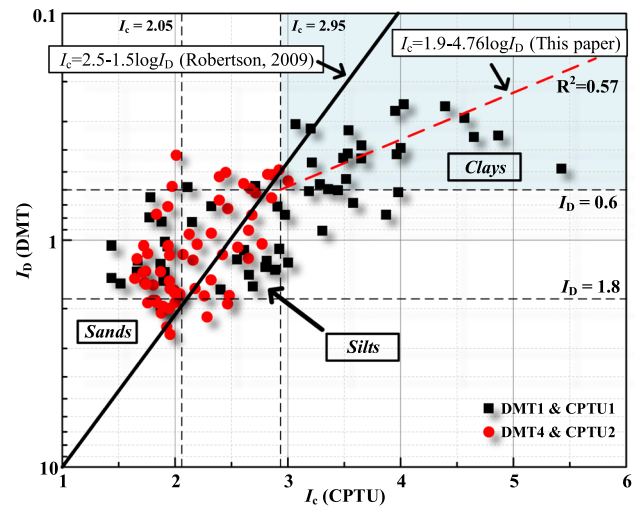


Fig. 14 Summary of measured values from adjacent CPT and DMT profiles of I_D versus I_c

$$\begin{cases} K_D = 0.03Q_{t1}^{1.06} + 2.05 \\ E_D/\sigma'_{v0} = 39.81Q_{t1}^{0.25} \end{cases} \text{ (South bank)} \tag{28}$$

$$\begin{cases} K_D = 7.54Q_{t1}^{1.97} + 1.19 \\ E_D/\sigma'_{v0} = 11.22Q_{t1}^{0.56} \end{cases} \text{ (North bank)} \tag{29}$$

5 Summary and conclusions

Piezocone penetration tests, dilatometer tests and a series of laboratory experiments conducted in Haimen-Taicang river-crossing tunnel project characterised the soil profile and estimated the primary geotechnical properties of both onshore and offshore soils. Based on the observations and analysis presented in this paper, the following conclusions can be drawn:

1. In the study area, the strata of both two riverbanks and riverbed has been presented as well as several physical and mechanical properties of each soil layer. After comparison, the soils on the south bank of the Yangtze River are consistent with that on the bottom of the river and quite different from that on the North Bank.
2. In general, soil classification methods originated from CPTU parameters seem to be more reliable than that based on DMT test. Two reasons may explain this: first, the testing data interval of DMT is larger. In this paper, silt-sand mixture is the main deposit, large testing interval brings deviation in matching the drilled soil layer with the soil layer identified by DMT. Second, DMT method only divides soils only based on

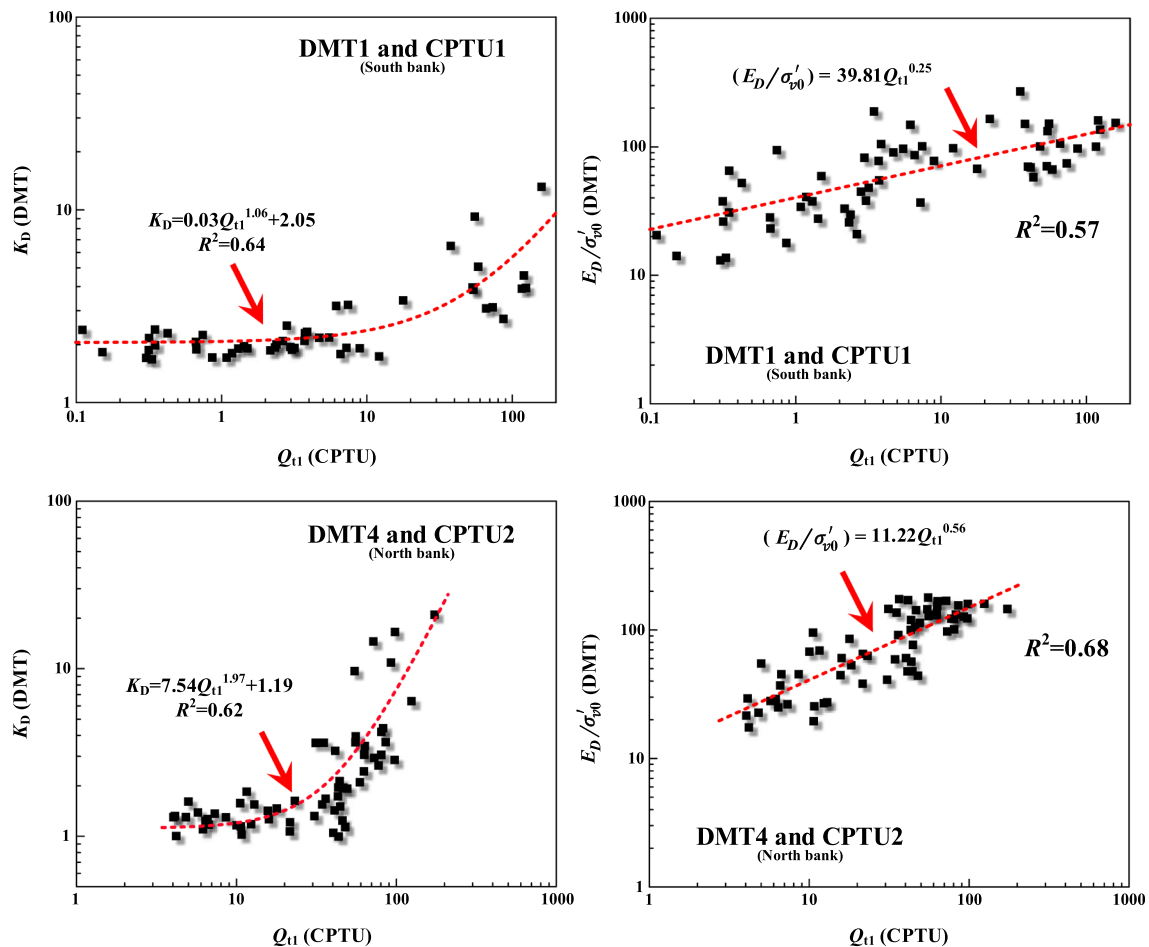


Fig. 15 Summary of measured values from adjacent CPT and DMT profiles of K_D versus Q_{t1} and E_D/σ'_{v0} versus Q_{t1}

clayey-, silty- and sandy- properties, and could not identify mixtures of various soils. The q_t – R_f chart has great performance in soil classification on onshore soils, and the Q_{t1} – B_q chart has the highest accuracy in identifying underwater soil types.

- For unit weight, undrained shear strength, constrained modulus, which can be estimated by both DMT and CPTU tests, this paper compares the accuracy of several empirical methods in predicting the above geotechnical parameters. For practice use, site-specific verification of each empirical relationship has been conducted and new forms of these relationships have been provided to improve the regional applicability.
- The correlations of CPTU and DMT data in both clayey and sandy soils were reviewed in detail. In order to perform site investigation as correctly as possible, local correlations between CPTU and DMT results were developed for further practical use.

Acknowledgements This paper was supported by National Natural Science Foundation of China for Distinguished Young Scholars (Grant No. 42225206).

Data availability All data or models generated or analyzed during this study appear in the submitted article.

References

- Ahmadi MM, Robertson PK (2005) Thin layer effects on the CPT q_c measurement. *Can Geotech J* 42(9):1302–1317. <https://doi.org/10.1139/t05-036>
- Ahmed SM, Agaiby SS (2021) Undrained shear strength assessment using piezocone and shear wave measurements. *Proc Inst Civ Eng Geotech Eng* 174(2):126–138. <https://doi.org/10.1680/jgeen.20.00090>
- Ansari Y, Merifield R, Sheng D (2014) A piezocone dissipation test interpretation method for hydraulic conductivity of soft clays. *Soils Found* 54(6):1104–1116. <https://doi.org/10.1016/j.sandf.2014.11.006>
- Baldi G, Bellotti R, Ghionna V, Jamiolkowski M, Marchetti S, Pasqualini E (1986) Flat dilatometer tests in calibration chambers. In: *Use of in situ tests in geotechnical engineering*, pp 431–446. ASCE
- Bol E, Önalp A, Özocak A, Sert S (2019) Estimation of the undrained shear strength of Adapazari fine grained soils by cone penetration test. *Eng Geol* 261:105277. <https://doi.org/10.1016/j.enggeo.2019.105277>

6. Cai GJ, Liu SY, Puppala AJ (2015) Consolidation parameters interpretation of CPTU dissipation data based on strain path theory for soft Jiangsu quaternary clays. *Mar Georesour Geotechnol* 33(4):310–319. <https://doi.org/10.1080/1064119X.2013.872742>
7. Cai GJ, Liu SY, Tong LY, Du GY (2010) Field evaluation of undrained shear strength from piezocone penetration tests in soft marine clay. *Mar Georesour Geotech* 28(2):143–153. <https://doi.org/10.1080/10641191003780906>
8. Chai JC, Sheng DC, Carter JP, Zhu HH (2012) Coefficient of consolidation from non-standard piezocone dissipation curves. *Comput Geotech* 41:13–22. <https://doi.org/10.1016/j.compgeo.2011.11.005>
9. Duan W, Cai GJ, Liu SY, Puppala AJ, Chen RF (2019) In-situ evaluation of undrained shear strength from seismic piezocone penetration tests for soft marine clay in Jiangsu, China. *Transp Geotech* 20:100253. <https://doi.org/10.1016/j.trgeo.2019.100253>
10. Ebrahimian B, Movahed V, Pasha AY (2012) Evaluation of undrained shear strength of marine clay using cone penetration resistance at South Pars field in Iran. *Ocean Eng* 54:182–195. <https://doi.org/10.1016/j.oceaneng.2012.07.018>
11. Golestani Dariani AA, Ahmadi MM (2018) Undrained shear strength and in situ horizontal effective stress from Piezocone penetration test measurements in clayey soils: new approach. *Int J Geomech* 18(9):04018097. [https://doi.org/10.1061/\(ASCE\)GM.1943-5622.0001210](https://doi.org/10.1061/(ASCE)GM.1943-5622.0001210)
12. Grabar K, Strelec S, Špiranec M, Dodigović F (2022) CPT-DMT correlations on regional soils from Croatia. *Sensors* 22(3):934. <https://doi.org/10.3390/s22030934>
13. Jefferies MG, Davies MP (1991) Soil classification by the cone penetration test. *Can Geotech J* 28(1):173–176
14. Liu SY, Cai GJ, Puppala AJ, Tu Q (2011) Prediction of embankment settlements over marine clay using piezocone penetration tests. *Bull Eng Geol Environ* 70(3):401–409. <https://doi.org/10.1007/s10064-010-0329-4>
15. Liu SY, Zou HF, Cai GJ, Zhang LM, Puppala AJ (2020) Piezocone penetration test-based site characterisation of Chong–Qi Bridge project, China. *Proc Inst Civ Eng Forensic Eng* 173(1):25–34. <https://doi.org/10.1680/jfoen.19.00014>
16. Liu XN, Shen JR, Yang M, Cai GJ, Liu SY (2022) Subsurface characterization of a construction site in Nanjing, China using ERT and CPTU methods. *Eng Geol* 299:106563. <https://doi.org/10.1016/j.enggeo.2022.106563>
17. Lunne T, Powell JJ, Robertson PK (2002) Cone penetration testing in geotechnical practice. CRC Press, Cambridge
18. Lutenege AJ (2006) Cavity expansion model to estimate undrained shear strength in soft clay from dilatometer. In: Proceedings of the second international flat dilatometer conference, Washington, DC, USA, pp 2–5
19. Marchetti S (1980) In situ tests by flat dilatometer. *J Geotech Eng* 106(3):299–321
20. Marchetti S, Crapps DK (1981) Flat dilatometer manual. Schmertmann and Crapps Inc., Gainesville
21. Marchetti S, Monaco P, Totani G, Calabrese M (2001) The flat dilatometer test (DMT) in soil investigations—a report by the ISSMGE Committee TC16. Official version approved by ISSMGE TC16 reprinted in Failmezger RA, Anderson JB (eds) Proceedings of the second international conference on flat dilatometer, Washington DC, 2–5 April 2006, pp 7–48
22. Mayne PW (2007) In-situ test calibrations for evaluating soil parameters. In: Characterization and engineering properties of natural soils, vol 3. Taylor & Francis Group, London, pp 1602–1652
23. Mayne PW (2016) Evaluating effective stress parameters and undrained shear strengths of soft-firm clays from CPTu and DMT. *Aust Geomech J* 50(4):27–55
24. Mayne PW, Peuchen J (2018) Evaluation of CPTU N_{kt} cone factor for undrained strength of clays. In: Hicks MA, Pisanò F, Peuchen J (eds) Cone penetration testing 2018—proceedings of the 4th international symposium on cone penetration testing (CPT'18), Delft, the Netherlands. CRC Press, Leiden, pp 423–428
25. Monaco P, Amoroso S, Marchetti S, Marchetti D, Totani G, Cola S, Simonini P (2014) Overconsolidation and stiffness of venice lagoon sands and silts from SDMT and CPTU. *J Geotech Geoenviron Eng* 140(1):215–227
26. Ouyang ZK, Mayne PW (2018) Effective friction angle of clays and silts from piezocone penetration tests. *Can Geotech J* 55(9):1230–1247. <https://doi.org/10.1139/cgj-2017-0451>
27. Pineda JA, Suwal LP, Kelly RB, Bates L, Sloan SW (2016) Characterisation of Ballina clay. *Géotechnique* 66(7):556–577. <https://doi.org/10.1680/jgeot.15.P.181>
28. Robertson PK (1990) Soil classification using the cone penetration test. *Can Geotech J* 27(1):151–158
29. Robertson PK (2009) CPT-DMT Correlations. *J Geotech Geoenviron Eng* 135(11):1762–1771. [https://doi.org/10.1061/\(ASCE\)GT.1943-5606.0000119](https://doi.org/10.1061/(ASCE)GT.1943-5606.0000119)
30. Robertson PK, Campanella RG, Gillespie D, Greig J (1986) Use of piezometer cone data. In: In-situ'86 use of in-situ testing in geotechnical engineering, GSP 6, ASCE, Reston, Va, Vol. 92. Specialty Publication, SM, pp 1263–1280
31. Robertson PK, Cabal KL (2010) Estimating soil unit weight from CPT. In: Proceedings of the 2nd international symposium on cone penetration testing (CPT'10), Huntington Beach, CA, 9–11 May 2010
32. Vesić AS (1972) Expansion of cavities in infinite soil mass. *J Soil Mech Found Div (ASCE)* 98(SM3):265–290
33. Vesić AS (1977) Design of pile foundations, NCHRP Synthesis No. 42, Transportation Research Board, National Academy Press, Washington, DC

Publisher's Note Springer Nature remains neutral with regard to jurisdictional claims in published maps and institutional affiliations.

Springer Nature or its licensor (e.g. a society or other partner) holds exclusive rights to this article under a publishing agreement with the author(s) or other rightsholder(s); author self-archiving of the accepted manuscript version of this article is solely governed by the terms of such publishing agreement and applicable law.